fibers

MDPI

Article

Influence of Fiber Volume Fraction and Fiber Orientation on the Uniaxial Tensile Behavior of Rebar-Reinforced Ultra-High Performance Concrete

Manish Roy [1], Corey Hollmann [2] and Kay Wille [1,*]

1 Civil & Environmental Engineering Department, University of Connecticut, 261 Glenbrook Road Unit 3037, Storrs, CT 06269-3037, USA

2 Michael Horton Associates, Inc., Branford, CT 06405, USA

* Correspondence: kay.wille@uconn.edu; Tel.: +1-860-486-2074

Received: 18 May 2019; Accepted: 18 July 2019; Published: 23 July 2019

check for updates

Abstract: This paper studied the influence of fiber volume fraction (V_f), fiber orientation, and type of reinforcement bar (rebar) on the uniaxial tensile behavior of rebar-reinforced strain-hardening ultra-high performance concrete (UHPC). It was observed that the tensile strength increased with the increase in V_f. When V_f was kept constant at 1%, rebar-reinforced UHPC with fibers aligned with the load direction registered the highest strength and that with fibers oriented perpendicular to the load direction recorded the lowest strength. The strength of the composite with random fibers laid in between. Moreover, the strength, as well as the ductility, increased when the normal strength grade 60 rebars embedded in UHPC were replaced with high strength grade 100 rebars with all other conditions remaining unchanged. In addition, this paper discusses the potential of sudden failure of rebar-reinforced strain hardening UHPC and it is suggested that the composite attains a minimum strain of 1% at the peak stress to enable the members to have sufficient ductility.

Keywords: UHPC; rebar; fiber; tension; orientation; composite; ductility

1. Introduction

This research focuses on the uniaxial tensile behavior of rebar-reinforced ultra-high performance concrete (reinforced UHPC). In an un-cracked state, reinforced UHPC under tensile loading can be assumed to behave elastically with perfect bond (Figure 1a). This is similar to conventional reinforced concrete (RC) under uniaxial tension. As the tensile load is increased, it leads to the development of micro cracks as soon as the matrix reaches its cracking strength locally (Figure 1b). For the purpose of this study, micro cracks are defined as any crack with an upper limit of 10 μm width; beyond this width limit, cracks are considered to be macro cracks [1]. In comparison to RC where the tensile load across the crack is only transferred by the rebar, reinforced UHPC allows the transfer of the tensile load across the crack by the combined effort of fiber-reinforcement and rebar. This crack-bridging effect of the fibers increases the composite stiffness beyond the tension stiffening effect of rebar reinforced concrete [2]. With a further increase in the tensile load, strain-hardening UHPC exhibits multiple cracking (Figure 1c). It is worth noting here that this phenomenon of multiple cracking differentiates strain-hardening cementitious composites (e.g., UHPC containing at least 1.5 vol.% steel fibers of aspect ratio 65 [3]) in its composite tensile behavior from conventional fiber reinforced concrete (FRC). The multiple cracking of the matrix continues with the increased tensile load until the tensile strength of UHPC is reached. Then the fiber-reinforced matrix starts softening, which leads to the development of a macro crack (Figure 1d). At this stage or with further increase in the tensile load, the yielding rebar starts strain-hardening, resulting in the formation of multiple macro cracks (Figure 1e) followed by rebar softening and ultimately, failure (Figure 1f).

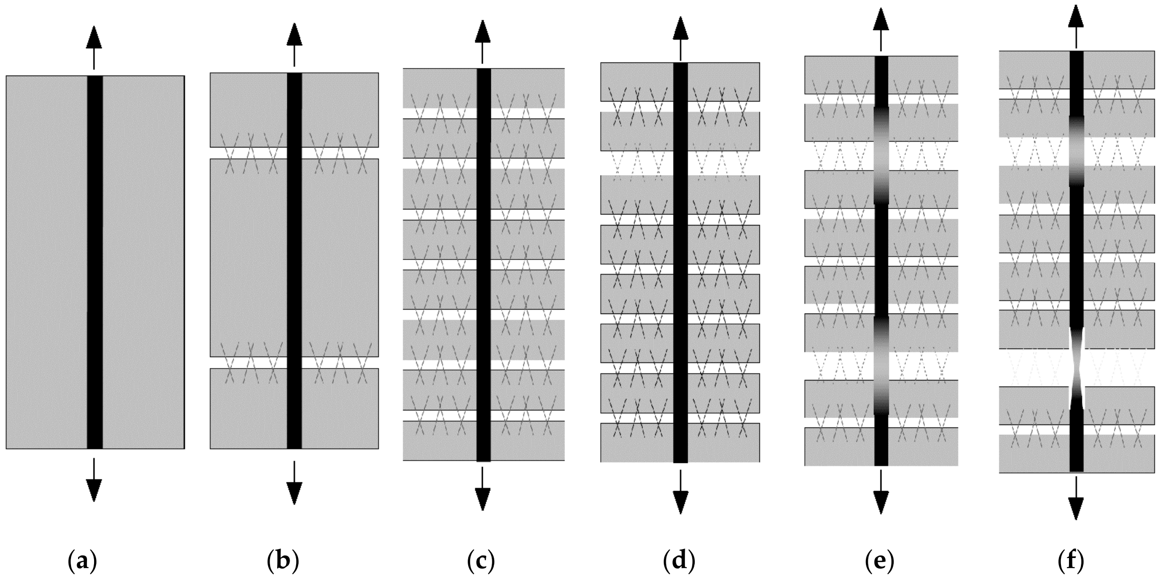

Figure 1. Mechanics of strain-hardening reinforced UHPC under tension (after [4]): (**a**) Uncracked; (**b**) Fiber bridging; (**c**) Multiple matrix cracking due to strain hardening; (**d**) Macro cracking due to matrix softening; (**e**) Multiple macro cracking due to rebar hardening; (**f**) Rebar failure/softening.

Figure 1 demonstrates how the fiber reinforcement influences the development of micro and macro cracks under increased tensile loading. The effect of fiber reinforcement is controlled by the type, the amount, and the orientation of fibers [5] present in the composite. The fiber reinforcement not only enhances the tensile load transfer along the load direction as illustrated in Figure 1, but it also improves the bond properties between the rebar and the fiber composite [6]. Under tensile loading, the bond between the matrix and the fibers, as well as the splitting cracks, develops along the load direction. Hence, fibers, oriented perpendicular to the load direction, improve the bond properties more effectively than that aligned with the load direction [7]. This phenomenon motivated the authors to investigate the effect of fiber orientation on the overall performance of reinforced UHPC under tensile loading.

Several researchers investigated the behavior of reinforced UHPC under tensile loading. Redaelli [8] performed direct tension tests on real-scale (160 mm × 160 mm cross-section with 1 m measurement length) UHPC dog bone-shaped specimens reinforced with ordinary steel bars (16 mm diameter). He found that the cracks opened at the serviceability-limit state were thin and closely spaced (spacing ~20 to 100 mm). He also observed that the tension-stiffening effect in reinforced UHPC was more pronounced than that in RC, resulting in a higher stiffness of the composite. Moreover, reinforced UHPC might have a positive financial impact due to the possible reduction in the amount of expensive steel fibers added to the matrix. Leutbecher and Fehling [9] showed that rebar reinforced UHPC with as low as 0.9% fiber volume fraction (V_f) could demonstrate strain-hardening behavior with very small crack spacing and crack widths, whereas a typical UHPC may require sufficiently large amount of fibers ($V_f > 1.5\%$) [8] on its own to achieve strain-hardening and favorable crack width. This is of significant importance because the amount of expensive steel fibers dominates the cost of UHPC. A significant reduction in V_f can result in a significant reduction in material cost. Kunieda et al. [10] conducted uniaxial tensile tests on reinforced ultra-high performance strain hardening cementitious composite (UHP-SHCC) specimens having compressive strength (f_c') of 95 MPa and 1.5% V_f. They observed that all the UHP-SHCC specimens showed strain-hardening behavior with multiple cracking. Similar experiments on rebar-embedded FRC, carried out by other researchers [11–13], showed favorable results with respect to crack spacing and crack width. A review of the aforesaid literature suggests that the interaction between rebar and concrete in RC or the interaction among rebar, concrete, and fibers in conventional FRC is well understood. However, the interaction between rebar and strain-hardening UHPC needs to be investigated further in order to understand the effect of strain-hardening characteristic on the composite tensile behavior.

2. Brittle Failure of Reinforced Strain-Hardening UHPC?

Strain-hardening UHPC is characterized by multiple cracking and significantly enhanced energy absorption capacity until failure [3]. Prima facie, reinforced strain-hardening UHPC is expected to behave as a highly ductile material due to the ductile behavior of both the fiber-reinforced matrix and the hardening rebar. However, the following conditions could lead to a rather brittle failure and thus, motivated this research to investigate further.

The softening behavior of strain-hardening UHPC is characterized by the formation and subsequent opening of a macro crack similar to that of FRC. If the softening behavior of the fiber-reinforced UHPC matrix (i.e., the slope of region A-B in Figure 2) and thus the decrease in force (ΔF_m) due to the decrease in stress resistance ($\Delta\sigma_m$) is more pronounced than the hardening behavior of the rebar (i.e., the slope of region C-D in Figure 2) and thus the increase in force (ΔF_r) due to the increase in stress resistance ($\Delta\sigma_r$), then opening of only one macro crack might lead to a local rebar failure (region E-F in Figure 2). In other words, if during softening, ΔF_m (decrease in force in the fiber-reinforced UHPC matrix) > ΔF_r (increase in force in the rebar) (Figure 3), then the load carrying capacity of the reinforced composite will be reached as soon as the first macro crack forms and hence, the formation of only one macro crack will lead to a sudden failure of the composite. This yield-point localization without forming other rebar yield points leads to a loss of ductility of the composite [14], which might pose a threat to the structure at the ultimate limit state [8].

In summary, one of the following two conditions occurs when the UHPC matrix reaches the peak tensile strength under uniaxial tensile loading:

$$\text{If } |\Delta F_m| < |\Delta F_r| \rightarrow \text{ formation of multiple macro cracks } \rightarrow \text{ increase in ductility} \quad (1)$$

$$\text{If } |\Delta F_m| > |\Delta F_r| \rightarrow \text{ formation of one macro crack } \rightarrow \text{ loss of ductility} \quad (2)$$

where

$$\Delta F_m = \Delta\sigma_m \times A_m \quad (3)$$

$$\Delta F_r = \Delta\sigma_r \times A_r \quad (4)$$

and A_m and A_r are the area of the matrix and the rebar, respectively.

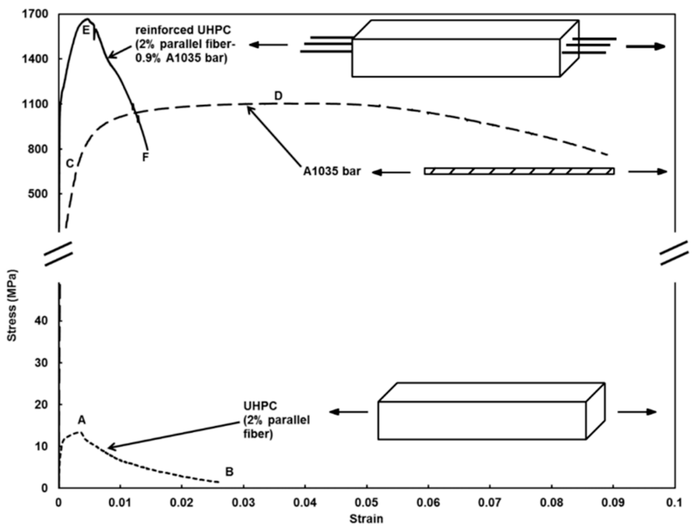

Figure 2. Comparison of stress versus strain curves of UHPC, reinforced UHPC, and reinforcement steel.

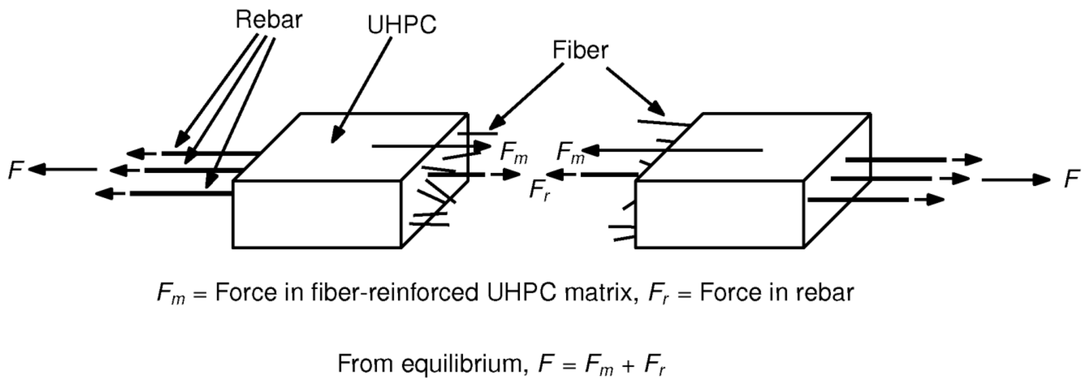

Figure 3. Reinforced UHPC during softening (idealized).

The multiple cracking of the matrix followed by the formation of one macro crack provides sufficient ductility to the composite for controlling cracks at the serviceability limit state. However, it is important that the composite has sufficient ductility to attain high strain levels at the ultimate limit state [9]. Improved ductility at high strain levels through tailored finer-reinforcement, accompanied by the formation of multiple macro cracks, would ensure the safety of the structure at the ultimate limit state. Leutbecher [15] recommended decreased fiber content and the use of rebar with pronounced hardening to achieve multiple macro cracks, similar to conventional RC. Redaelli [8] suggested the use of rebar with enhanced and continuous strain-hardening property in order to improve ductility. Sturwald and Fehling [16] proposed an increased amount of rebar reinforcement at higher fiber dosages in order to make bar hardening more pronounced than the softening behavior of the fibers. Thus, for ultimate limit-state design, the influence of the fibers, as well as the rebar reinforcement, has to be considered to attain a ductile composite behavior at failure [17]. Although other researchers [8,18,19] have encountered a similar problem of strain localization at the ultimate limit-state, research on the effect of orientation and amount of fibers in UHPC as well as the type of rebar reinforcement has been very limited [20]. Hence, an effort has been made in this research to characterize the behavior of rebar-embedded strain-hardening UHPC under uniaxial tension with a major focus on the effect of type of rebar reinforcement and the amount and orientation of fibers.

3. Materials and Methods

3.1. Materials

3.1.1. Rebar–Characterization

Two different grades of uncoated deformed #3 (nominal diameter ≈ 9.5 mm) steel rebar, viz. normal strength grade 60 and high strength grade 100, were used in the experiment. The grade 60 rebar had yield strength (f_y) of 415 MPa and conformed to the specifications of ASTM A615 [21]. It will hereinafter be referred to as A615. The grade 100 rebar conformed to the specifications of ASTM A1035 [22] and will hereinafter be referred to as A1035. Due to its high yield strength (f_y = 700 MPa), A1035 facilitates reduction in the quantity of reinforcement in a structure provided sufficient bond is present. This, in turn, improves the constructability. Furthermore, by virtue of its low amount of carbon (≤0.15% by weight) and chromium (~8–10% by weight), A1035 is also highly corrosion-resistant enabling structures to be more durable and thereby decreasing the life cycle cost.

Uniaxial tensile tests were carried out in accordance with the specifications of ASTM A370 [23] on three bars each for A615 and A1035. Table 1 shows the average key results from the tests. The stress versus strain curves of all the specimens along with the average curves for both A615 and A1035 are shown in Figure 4. The figure shows that A1035 does not have a well-defined yield plateau in contrast to that of ASTM A615 bar [7]. Similar behavior of A1035 was also reported by Seliem et al. [24].

Table 1. Rebar average test data (Adapted from [7]).

Bar Type	Modulus of Elasticity E_s (MPa)	Yield Stress f_y (MPa)	Ultimate Stress f_t (MPa)	f_t/f_y
A615	208,078	457	719	1.57
A1035	221,858	700	1102	1.57

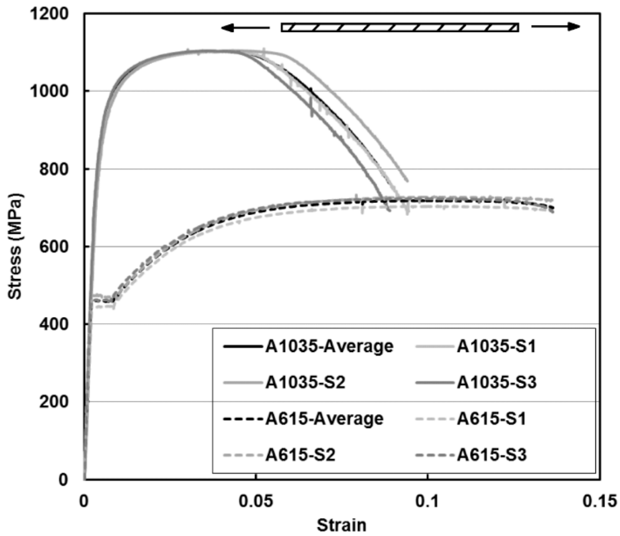

Figure 4. Average stress versus strain curves of A615 and A1035 rebar used in this research (Adapted from [7]).

3.1.2. UHPC–Material Design and Characterization

The mixture proportions of the proprietary premix of UHPC used in the experiment are shown in Table 2. The Premix contained an undisclosed amount of silica fume, ground quartz, sand, and cement. The fibers used were high strength steel fibers with yield strength in excess of 2000 MPa and an aspect ratio of 65 (13 mm in length and 0.2 mm in diameter). The fibers had a slightly deformed mid-section (Figure 5 for reference). The mixing procedure has been outlined in [7].

Table 2. Mixture proportions and compressive strength of UHPC (Adapted from [7,25]).

Mixture Proportions		Compressive Strength (MPa)		
Ingredients	Quantity (kg/m^3)	Age of Concrete During Testing (day)	0% Fiber	2% Fiber
Premix	2195	7	126.9	122.6
Water	120	14	161.0	162.0
Superplasticizer	30	28	172.7	176.1
Steel Fibers (2%)	156	-	-	-

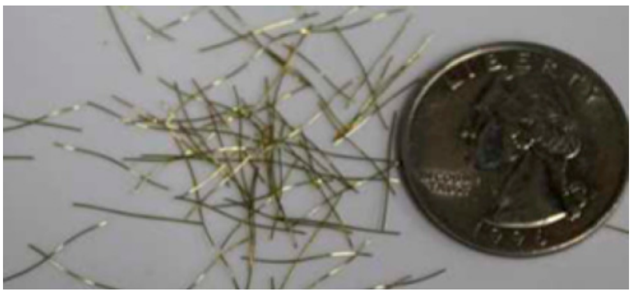

Figure 5. Steel fibers with slightly deformed mid-section [7].

Compression testing of UHPC was carried out on cylindrical specimens (76 mm diameter × 152 mm height) as per modified ASTM C39 [26] using a 1780 kN load frame. Three specimens were cast and tested at 7, 14, and 28-days and the average compressive strength values are reported in Table 2. The casting procedure and the testing procedure have been outlined in detail in [7].

Direct tension tests of UHPC were performed on 25 mm × 50 mm × 406 mm long prismatic specimens after 14 days of casting. Three different casting methods, viz., Parallel, RandomA, and RandomB were used. In "Parallel" casting method, a scoop was used to pour the UHPC back and forth along the length of the mold in small layers at a pace fast enough to align the fibers. The "RandomA" method consisted of pouring the UHPC in the center of the mold and allowing the material to flow to the ends. In "RandomB" method, the UHPC was placed at one end of the mold and allowed to flow to the opposite end. Four different V_f values, viz., 0%, 1%, 2%, and 3% were used. At least three specimens were cast for each series. However, one specimen in each "2% fiber-parallel" and "3% fiber-parallel" series broke within the grip during testing and was rendered invalid. Hence, the average strength for each of those two series was calculated based on the results of two specimens. The tests were performed using a 1780 kN load frame. A picture of the test set-up is shown in Figure 6. Loading was applied by displacement controlled method at a rate of 0.5 mm/min. The testing procedure is explained in [7]. The average maximum tensile stress values are plotted in Figure 7.

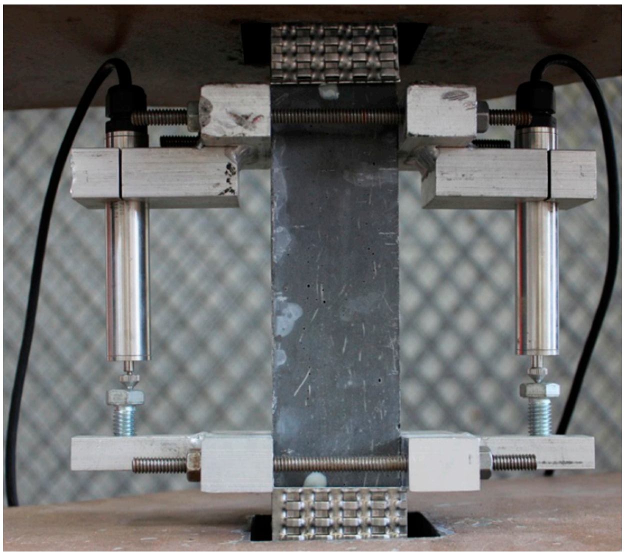

Figure 6. Test set-up for the uniaxial tensile test of UHPC [7].

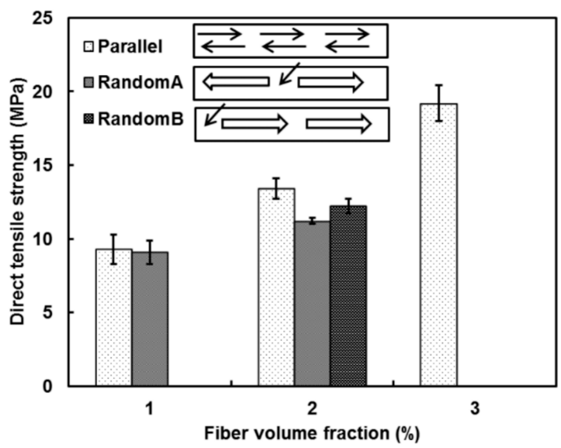

Figure 7. Average maximum stress of UHPC under uniaxial tension [7].

Figure 8a shows the average stress versus strain curves up to the ultimate stress for UHPC with parallel fibers corresponding to different fiber volume fractions; whereas Figure 8b shows the stress versus crack opening displacement relationship of the same materials in the softening zone. Similar curves are shown in Figure 9a,b for UHPC with random fiber orientation.

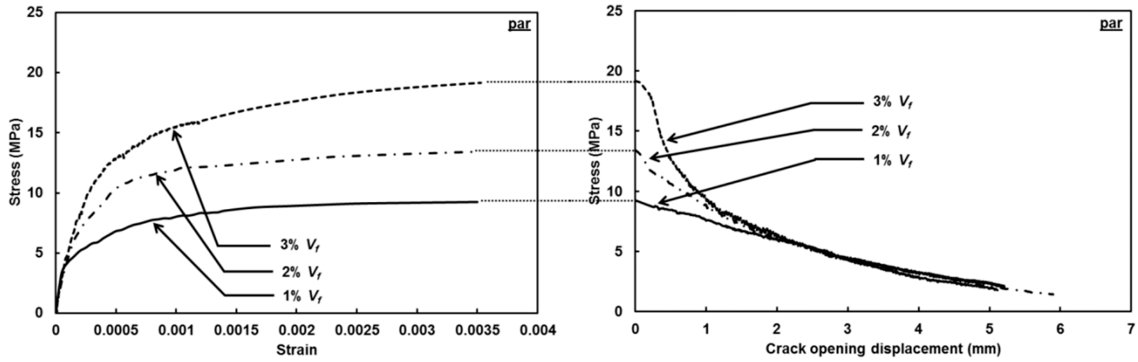

(**a**) (**b**)

Figure 8. Average curves for UHPC with parallel fiber orientation under uniaxial tension: (**a**) Stress versus strain; (**b**) Stress versus crack opening displacement.

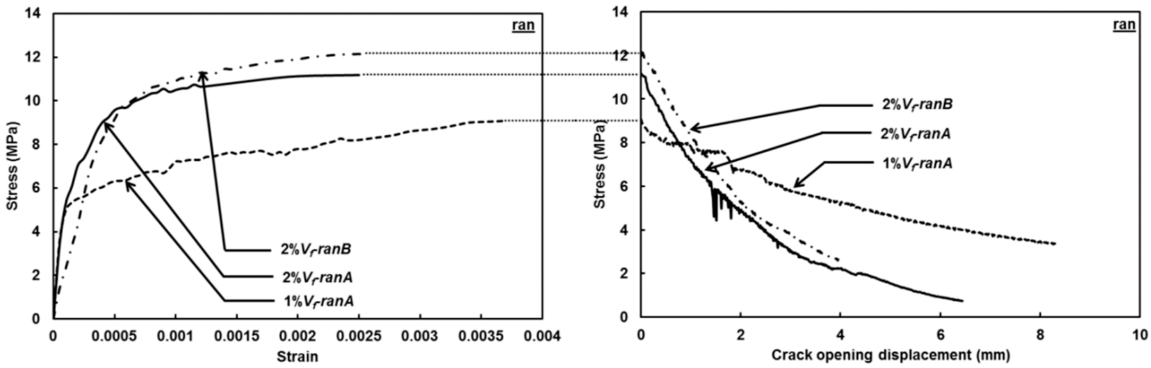

(**a**) (**b**)

Figure 9. Average curves for UHPC with random fiber orientation under uniaxial tension: (**a**) Stress versus strain; (**b**) Stress versus crack opening displacement.

3.2. Uniaxial Tensile Test of Rebar-Reinforced UHPC

3.2.1. Test Specimen Design

A test set-up for rebar-reinforced strain-hardening UHPC under uniaxial tension is more complicated in nature than a test set-up for ordinary RC because the fibers in strain-hardening UHPC allow the composite to reach a peak load greater than that of the rebar itself. This means that a single bar run through the axis of the specimen and gripped on both ends would fail outside of the specimen as the exposed bar is the weakest portion of the specimen. In order to prevent failure outside of the specimen, different researchers have used different specimens ranging from dog-bone shaped [8,27] to heavier reinforced ends [10,28,29] to a combination of both [4,11,30]. In the present study, the test specimen was designed around the need to run tests using wedge grips and therefore, dog-bone specimens were ruled out. Instead, prismatic specimens (76 mm × 102 mm × 1020 mm long) were used with extra reinforcement added to the ends. A line sketch of the specimen with dimensions is shown in Figure 10a and an assembled mold is shown in Figure 10b.

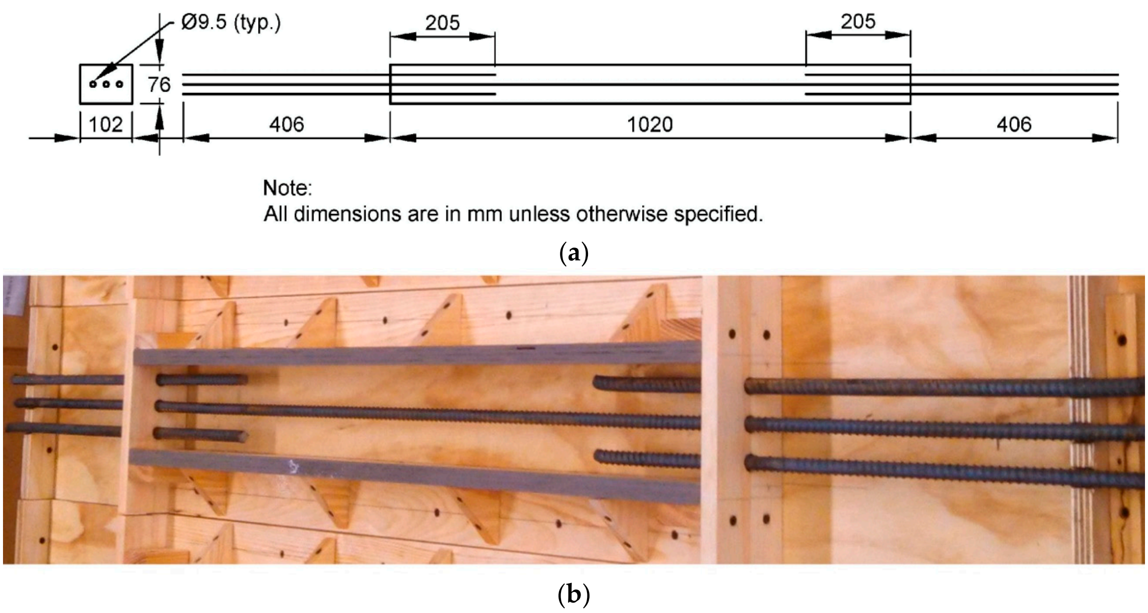

Figure 10. Specimen preparation: (**a**) Line sketch of the specimen; (**b**) Assembled mold.

3.2.2. Test Matrix

A total of sixteen different series based on volume fraction and orientation of fiber and type of rebar were tested under uniaxial tension. The number of specimen in each series is listed in Table 3. Due to the large size of the specimens, only one specimen was cast in each series except for a few selected series.

Table 3. Test matrix.

Fiber Volume Fraction	Fiber Orientation	Parallel		Perpendicular		Random	
	Rebar [1] Type	A1035	A615	A1035	A615	A1035	A615
V_f	0.5	1	1	-	-	1	-
	0.75	1	2	-	-	-	-
	1.0	2	2	1	1	1	1
	2.0	1	2	-	-	1	-
	3.0	1	-	-	-	1	-

[1] #3 (nominal diameter ≈ 9.5 mm).

3.2.3. Specimen Preparation

Before pouring of concrete, a light mineral oil was applied to the inside of the formwork and then the smaller side bars were set in place (Figure 11i). In order to align the fibers parallel to the load direction, concrete was poured back and forth along the length of the formwork starting from one end and going to the other (Figure 11ii,iii,v–viii). The middle bar was put in place once four layers of concrete were cast (Figure 11iv). For the perpendicular fiber orientation, the pouring was done orthogonal to the applied load. A similar casting principle to pre-align the fibers was used in [7]. For random fiber orientation, UHPC was poured at random spots throughout the formwork not giving too much time for it to flow before another spot near it was filled. This method prevented the fibers from aligning along a certain direction. No compaction was necessary as the UHPC material used in this study was self-compacting. All specimens were stripped of formwork after 48 h of casting, wrapped in plastic, and kept at room temperature until the 14-day testing time.

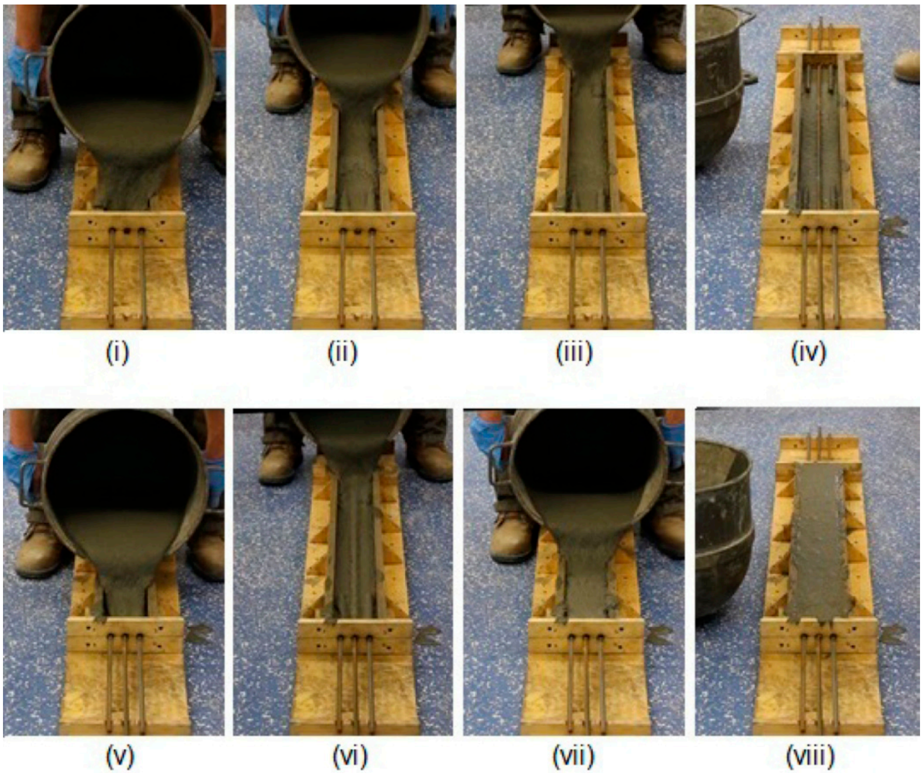

Figure 11. Casting sequence for parallel fiber orientation: (**i–iii**) UHPC is being poured back and forth from one end to the other to align the fibers; (**iv**) The pullout bar and the support bar are placed; (**v–vii**) UHPC is being poured back and forth from one end to the other to align the fibers; (**viii**) Pouring of UHPC is completed.

3.2.4. Testing

Before testing, the specimen was set up into the non-hydraulic wedge grips of a 1780 kN load frame. A set of two LVDT was attached to the custom holders that were pinhead-screwed to the specimen at each end (where the side bars stopped), so as to have a 610 mm long measurement length. The test set-up is shown in Figure 12. The tests were carried out using displacement control mechanism at the rate of 2 mm/min and force versus displacement of each LVDT was recorded. Water was rubbed onto the surface of the specimen to aid in viewing cracks.

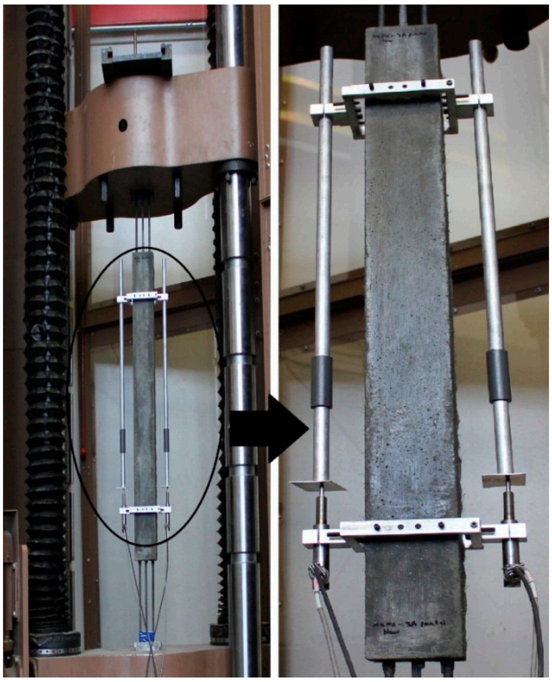

Figure 12. Test set-up with load frame and LVDT holder.

4. Results and Discussion

4.1. Peak Stress and Calculated UHPC Contribution

The peak stress of the composite is related to the rebar area and thus is calculated using Equation (5).

$$\sigma_{comp} = \frac{F_{peak}}{\pi {r_b}^2} \quad (5)$$

where F_{peak} is the maximum force reached by the composite and r_b is the radius of the rebar. Equation (6) shows the formula using which the UHPC contribution (σ_{uhpc}) has been determined.

$$\sigma_{uhpc} = \frac{(\sigma_{comp} - f_t)\pi {r_b}^2}{(A_c - \pi {r_b}^2)} \quad (6)$$

where f_t is the ultimate strength of rebar and A_c is cross-sectional area of the reinforced UHPC specimen.

4.1.1. Effect of V_f

The average peak stress values along with the calculated UHPC contribution for UHPC with embedded rebars are plotted against the fiber volume fractions in Figure 13a–c. It can be seen from Figure 13a that the peak stress of UHPC with parallel fibers and one A1035 reinforcement bar increases by 10%, 13%, and 36% when the V_f is increased from 0.5% to 0.75%, 1%, and 2%, respectively. The peak stress for 3% V_f is almost the same as that for 2% V_f. In case of UHPC with randomly oriented fibers and one A1035 rebar (Figure 13b), the peak stress is increased by 6%, 12%, and 21% when the V_f is increased from 0.5% to 1%, to 2%, and 3%, respectively. The peak stress in Figure 13c (with parallel fibers and one A615 rebar) increases by 14%, 28%, and 95% when the V_f is increased from 0.5% to 0.75%, 1%, and 2%, respectively. The contribution of UHPC in all the three graphs follows a similar trend as that of the composite, i.e., with the increase in V_f, the UHPC contribution increases. Since fibers transfer the tensile forces across cracks, higher fiber volume fraction increases the probability of the number of fibers crossing the cracks, thereby increasing the load carrying capacity of UHPC as well as the composite. In all the three figures, the peak stress of the composite is much higher than the corresponding ultimate stress in rebar. This is due to the superimposed crack-bridging effects of the fibers in UHPC and tensile stress in the reinforcement bars, leading to a composite stress that is higher than the ultimate strength of the rebar. This is one significant advantage of using reinforced UHPC instead of ordinary RC as in the case of RC, the stress of RC follows closely the stress in rebar once the matrix softens. Similar observation was also made by Redaelli [8].

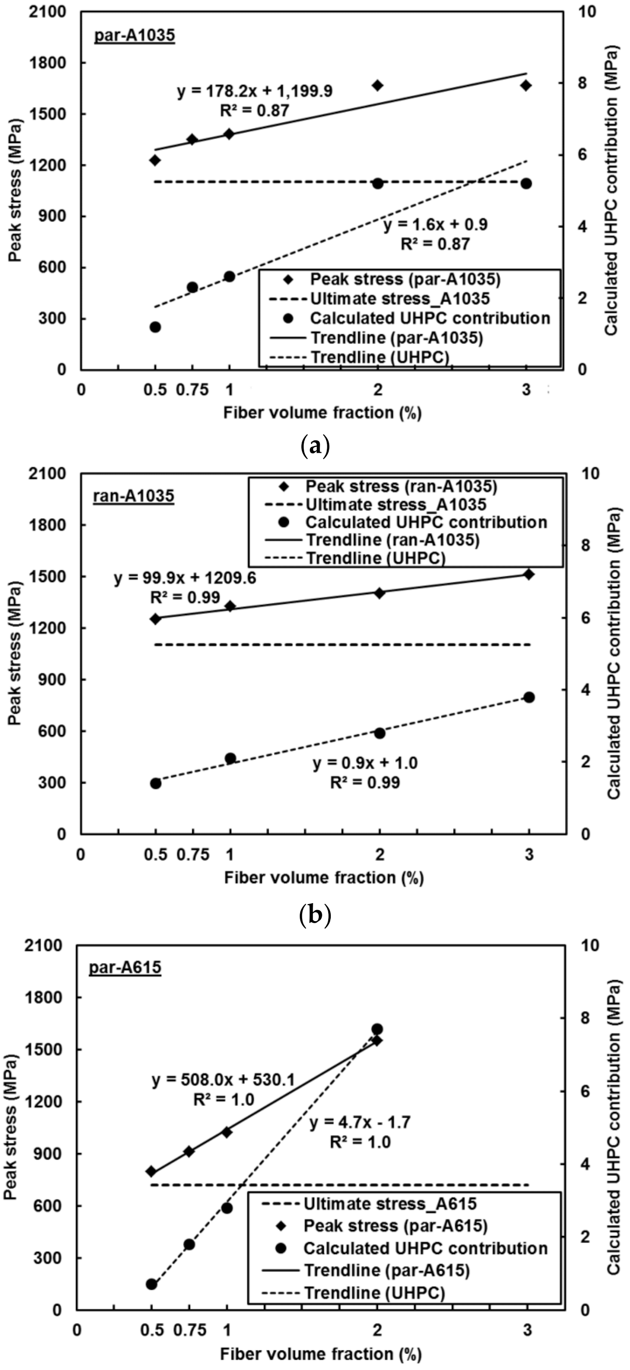

(c)

Figure 13. Effect of volume fraction on the peak stress of reinforced UHPC and on the UHPC contribution: (**a**) A1035 bars with parallel fiber orientation; (**b**) A1035 bars with random fiber orientation; (**c**) A615 bars with parallel fiber orientation.

4.1.2. Effect of Fiber Orientation

The effect of fiber orientation for reinforced-UHPC with 1% fibers is shown in Figure 14a (with A1035 bar) and Figure 14b (with A615 bar). In Figure 14a, the composite with random and parallel fiber orientation register an increase in peak stress by 9% and 14%, respectively, compared to that with perpendicular fiber orientation. In case of A615 bars (Figure 14b), the peak stress of the composite is increased by 4% and 37% when the fiber orientation is changed from perpendicular to random and from perpendicular to parallel, respectively. The calculated UHPC contribution follows a similar trend in both the figures. Since the specimens were subjected to uniaxial tension, the composite with fibers arranged parallel to the applied load had the highest probability of fibers crossing the cracks compared to the composites with random and perpendicular fiber orientation, thereby registering the maximum peak stress.

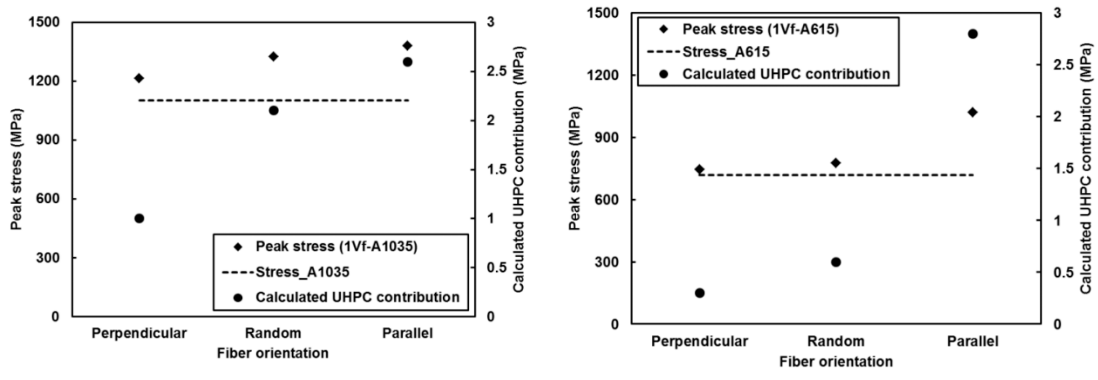

(**a**) (**b**)

Figure 14. Effect of fiber orientation (V_f = 1%) on tensile behavior: (**a**) A1035 bars; (**b**) A615 bars.

4.1.3. Effect of Rebar Type

Figure 15 shows the effect of rebar type on the uniaxial tensile behavior of the composite with parallel fiber orientation. It can be seen from the figure that the average peak stress of the composite with A1035 bars are 54%, 48%, 35%, and 7% higher than that with A615 bars for V_f = 0.5%, 0.75%, 1%, and 2%, respectively. Since A1035 bars have higher yield stress and ultimate stress than A615 bars, the composite with A1035 bars registers higher peak stress before the start of softening compared to that with A615 bars for a particular V_f and fiber orientation.

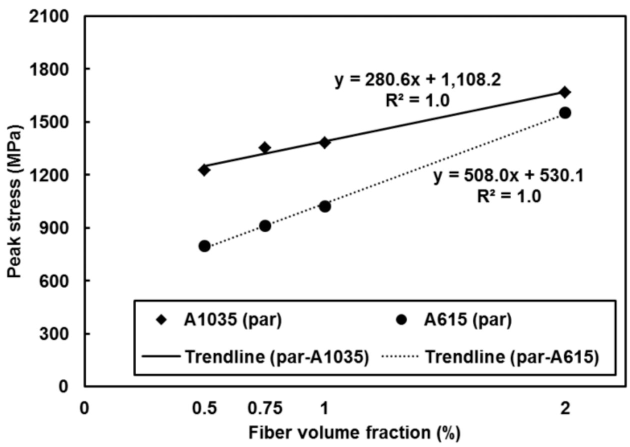

Figure 15. Effect of rebar type on the tensile behavior (parallel fiber orientation).

4.2. Stress versus Strain Response

In addition to the peak stress values discussed above, the stress versus strain response of the composite under uniaxial tension is analyzed here. The stress versus strain curves presented in this paper represent the calculated average curve of each series, which is obtained by averaging the interpolated stress values of different specimens at regular strain intervals. For example, Figure 16 shows the average stress versus strain curve of the composite with 1% fibers arranged parallel to the load direction and reinforced with A1035 bars. It also shows the modulus of the composite in the elastic region (E_c) for the average curve and that in the strain-hardening region (E_h) along with the maximum stress (σ_{pc}) and the strain at the maximum stress (ϵ_{pc}).

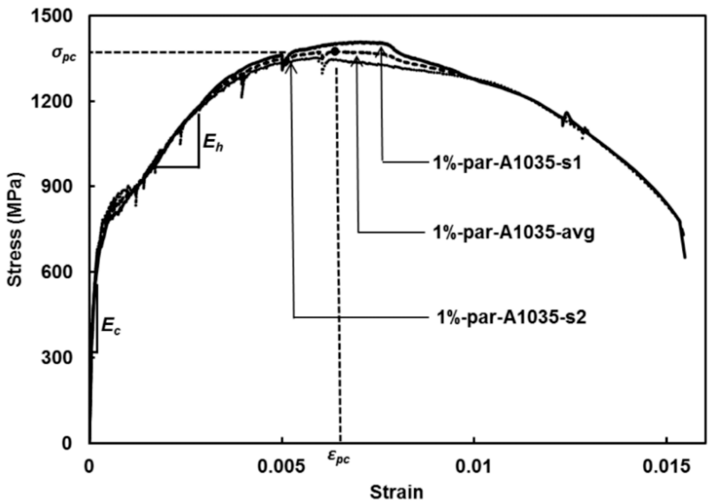

Figure 16. Typical variation of stress versus strain response of one test series.

4.2.1. Effect of V_f

Figure 17a–c show the effect of fiber volume fraction on the stress versus strain response of the composite with A1035 bars and parallel fiber orientation, with A1035 bars and random fiber orientation, and with A615 bars and parallel fiber orientation, respectively. It is evident from the aforesaid figures that the strain-hardening modulus (E_h) increases with the increase in fiber volume fraction. This is due to the improvement in the crack-bridging effect with the increase in V_f, thereby registering higher stresses at lower strains. However, the composite with A1035 rebar loses its ductility (defined as the strain at the peak stress) when V_f is increased further beyond a particular value (e.g., 0.75% for parallel fibers (Figure 17a) and 1% for random fibers (Figure 17b)). This is because the softening of UHPC becomes more pronounced with the increase in V_f as compared to the hardening of A1035 rebar. For example, in Table 4, ΔF_m for 1%-par-A1035 specimen increases from 1.9 kN to 5.7 kN with the increase in crack width from 0.15 mm to 0.4 mm (see exposure class [31]) based on the measured stress versus crack-width opening relationship of the UHPC. However, the value of ΔF_m is still lower than ΔF_r even at a higher crack width and thus leading to a ductile behavior. But in case of 3%-par-A1035 specimen, ΔF_m exceeds with 40 kN the value of $\Delta F_r = 28.5$ kN when the crack width is 0.4 mm. Hence, the specimen starts losing ductility as the crack width increases and becomes unstable as soon as ΔF_m surpasses ΔF_r. It is worthwhile to note the difference between material ductility and structural ductility here. Even though UHPC with fibers and steel rebar materials are separately considered to be ductile under tensile loads, a combination of these two materials may not always impart ductility to the resulting structure as evidenced here and hence, shows the importance of this study. For the composite with A615 bars (Figure 17c), ductility reduces when V_f is increased from 0.5% to 0.75% but beyond $V_f = 0.75\%$, ductility does not depend as such on V_f. Since A615 bar has a much lower yield strength as well as ultimate strength as compared to A1035 bars, the composite fails due to yield point localization.

Table 4. Force mechanism for the stress versus strain response.

Specimen	ΔF_r (kN) [a]	ΔF_m (kN) [b]	Crack Width (mm)	
1%-par-A1035	28.5	1.9	0.15 [c]	$\lvert\Delta F_m\rvert < \lvert\Delta F_r\rvert$ (Equation (1))
1%-par-A1035	28.5	5.7	0.4 [d]	$\lvert\Delta F_m\rvert < \lvert\Delta F_r\rvert$ (Equation (1))
3%-par-A1035	28.5	5.1	0.15 [c]	$\lvert\Delta F_m\rvert < \lvert\Delta F_r\rvert$ (Equation (1))
3%-par-A1035	28.5	40.0	0.4 [d]	$\lvert\Delta F_m\rvert > \lvert\Delta F_r\rvert$ (Equation (2))

[a] $\Delta F_r = \left(f_t - f_y\right)A_r$. [b] $\Delta F_m = \left(f_t' - \sigma_w\right)A_m$; σ_w is the stress in UHPC at a specific crack width (w) (Figure 8). [c] seawater; wetting and drying (Exposure data from [31]), [d] Dry air or protective membrane (Exposure data from [31]).

Recommendation for V_f

In reinforced concrete design, the steel reinforcement bars are assumed to attain a minimum strain of 0.5% in order to have a tension-controlled design such that the compression load is carried by the concrete and the tensile load is carried by the rebars alone. In order for the fibers in the UHPC to carry a part of the tensile load in case of rebar-reinforced UHPC structural members (utilizing the high tensile strength of UHPC), it is suggested that the composite attains a minimum strain of 1% at the peak stress enabling the members to have sufficient ductility. In Figure 17d, the strain at peak stress is plotted against V_f for the composite specimens. If 1% strain at the peak stress is considered as the threshold value for ductility, it can be recommended that UHPC with a low fiber volume faction (~0.5–0.75%) should be used in conjunction with strain-hardening rebars (such as A1035 bars) in order to achieve ductility for 0.9% reinforcement ratio.

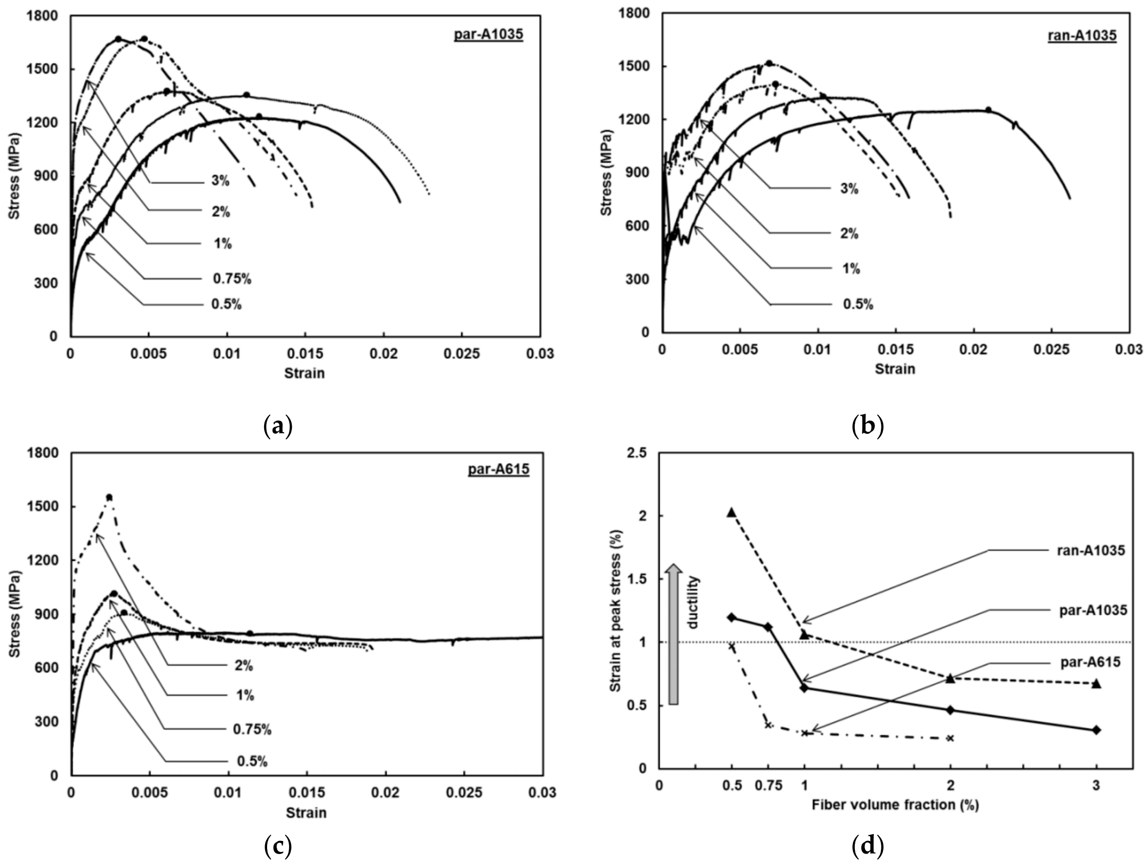

Figure 17. Effect of V_f on stress versus strain response: (**a**) A1035 bars with parallel fiber orientation; (**b**) A1035 bars with random fiber orientation; (**c**) A615 bars with parallel fiber orientation; (**d**) Ductility vis-à-vis fiber volume fraction.

4.2.2. Effect of Fiber Orientation

The effect of orientation of the fibers on the stress versus strain response is shown in Figure 18a for 1% V_f and A1035 rebars and in Figure 18b for 1% V_f and A615 rebars. In both the cases, the strain-hardening modulus registers the highest value when the fibers are aligned with the load direction and the lowest value when the fibers are arranged perpendicular to the load direction. These results confirm that the crack bridging effect is most effective when fibers are oriented parallel to the applied tensile load and the least effective when they are perpendicular to the load direction. However, the bond between UHPC and the rebar is better when the fibers are perpendicular to the load direction rather than parallel [7]. This explains the improvement in ductility for the composite with A1035 bars when the fiber orientation is changed from parallel to perpendicular with respect to the load direction (Figure 18a). In case of the composite with A615 bars (Figure 18b), the perpendicular fiber orientation registers a much higher strain at the peak stress (0.030) compared to the other two orientation types (0.003 for parallel and 0.006 for random).

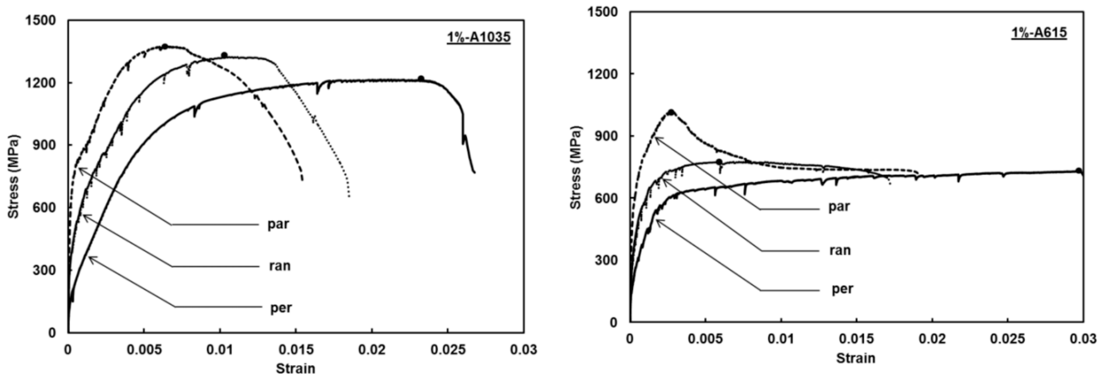

(**a**) (**b**)

Figure 18. Effect of fiber orientation on the stress versus strain response: (**a**) A1035 bars with 1% fibers; (**b**) A615 bars with 1% fibers.

4.2.3. Effect of Rebar Type

The effect of rebar type on the stress versus strain response of the composite with parallel fibers is shown in Figure 19. Since the modulus of A1035 bars and A615 bars are identical before yielding of A615 bars (Figure 4), the stiffness of the composite until softening of A615 bars is the same, given all other parameters remaining unchanged. However, the peak stress values of the composite with A1035 bars are higher than that with same-diameter A615 bars because of the higher ultimate strength of A1035 bars as compared to A615 bars. Also, the ductility of the composite with A1035 bars is better than that with A615 bars for a particular V_f.

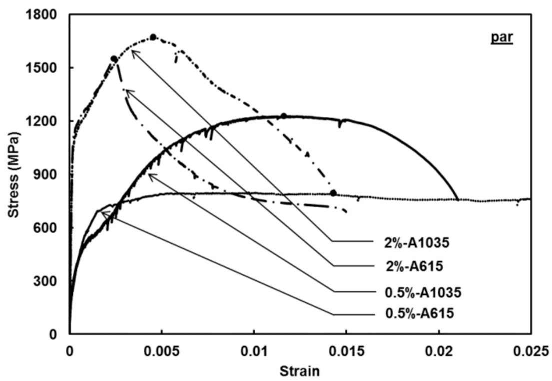

Figure 19. Effect of rebar type on stress versus strain response.

4.3. Failure Pattern

4.3.1. Effect of V_f

One representative failure pattern at rupture for each of the fiber volume fractions, viz. 0.5%, 1%, 2%, and 3% for a particular series (A1035 rebars with random fiber orientation) is shown in Figure 20a. The multiple macro cracks due to rebar-hardening are visible in this figure. In Figure 20b, the number of micro cracks per 600 mm at rupture as well as the macro cracks is plotted against V_f for the same series. It can be seen from this figure that the number of micro cracks increases due to crack-bridging as the fiber volume fraction increases. However as expected, the number of macro cracks decreases as V_f increases and thus the composite loses its ductility as V_f increases.

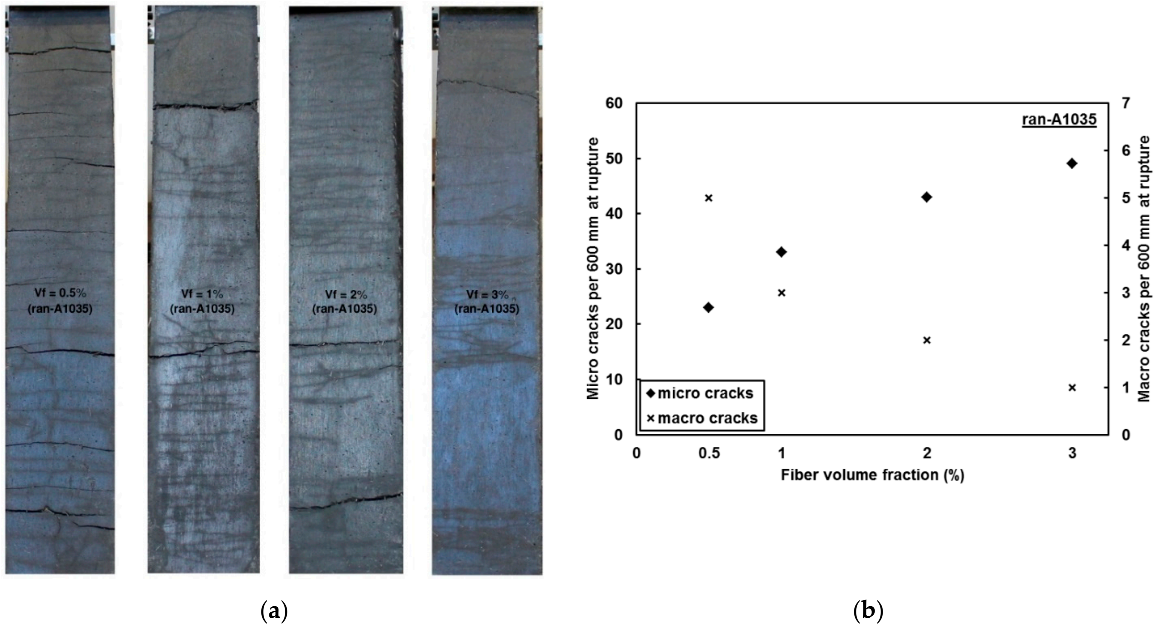

Figure 20. Failure of specimens w.r.t. fiber volume fraction: (**a**) Failure patterns; (**b**) Number of cracks.

4.3.2. Effect of Fiber Orientation

Figure 21a shows the representative failure patterns for different types of fiber orientation for the series with A1035 rebars and 1% fiber volume fraction, whereas Figure 21b shows the variation in number of micro cracks as well as macro cracks vis-à-vis the fiber orientation for the same series. It is evident from these two figures that the number of micro cracks is the highest in case of parallel fiber orientation due to the effective crack bridging. In case of perpendicular orientation, the fibers were aligned perpendicular to the load direction and hence, were not effective in crack bridging. As a result, the number of micro cracks in this case is the lowest among the three; however, the number of macro cracks is the highest in case of perpendicular fiber orientation due to improved ductility owing to better bonding and reduced ΔF_m.

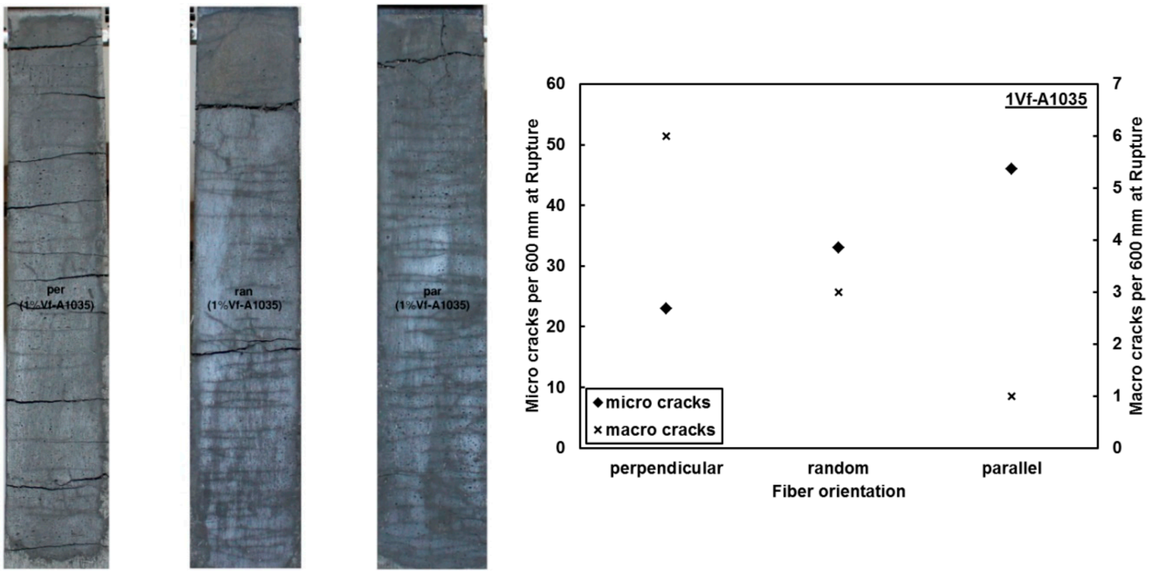

(**a**) (**b**)

Figure 21. Failure of specimens w.r.t. fiber orientation: (**a**) Failure patterns; (**b**) Number of cracks.

4.3.3. Effect of Rebar Type

The failure patterns and the number of micro/macro cracks per 600 mm for two different types of rebars are shown in Figure 22a,b, respectively. Both the specimens had 1% fibers oriented randomly with respect to the load direction. It can be seen from Figure 22a that the specimen with A615 bars has only one macro crack but the specimen with A1035 bars has multiple macro cracks due to better ductility. The number of micro cracks is also higher in case of A1035 bars, which is supported by Figure 22b.

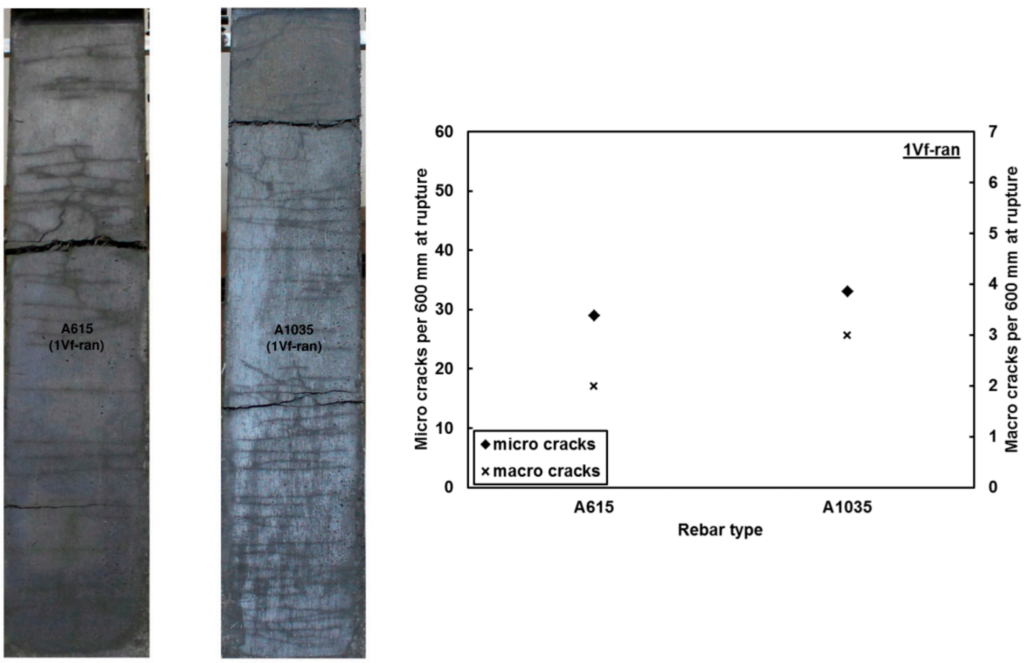

(**a**) (**b**)

Figure 22. Failure patterns w.r.t. rebar type (specimens with 1% fiber volume fraction and random fiber orientation): (**a**) Failure patterns; (**b**) Number of cracks.

5. Conclusions

Amid the growing interest in the application of rebar-reinforced ultra-high performance concrete (UHPC) in the US, the present study investigated the influence of the type of rebar reinforcement and the amount and orientation of fibers on the uniaxial tensile behavior of rebar-reinforced strain-hardening UHPC. The UHPC used in this study had a 14-day compressive strength of 162.1 MPa (28-day strength = 176.1 MPa) and a 14-day post-cracking uniaxial tensile strength of 13.4 MPa (with 2% fiber). The discrete steel fibers (aspect ratio = 65) imparted strain-hardening property accompanied by multiple cracking to the UHPC. Two different grades of uncoated deformed #3 (nominal diameter ≈ 9.5 mm) steel rebar, viz. normal strength grade 60 (f_y = 415 MPa) and high strength grade 100 (f_y = 700 MPa), were used in the experiment. A total of sixteen different series based on volume fraction and orientation of fiber and type of rebar were tested under uniaxial tension.

The conclusions from the uniaxial tests are summarized below:

- In general, the composite tensile strength increased with the increase in fiber volume fraction for a given rebar type and fiber orientation.
- For a given rebar type and fiber volume fraction, the UHPC with fibers oriented parallel to the load direction showed the highest peak tensile stress and the UHPC with fibers oriented perpendicular to the load direction recorded the lowest peak stress. The peak stress values with random fibers laid in between.
- UHPC with A1035 rebars recorded higher tensile stress as compared to UHPC with A615 rebars for a particular fiber volume fraction and parallel orientation of fibers.
- Average stress versus strain curves showed that the modulus of the composite in the strain-hardening region increased with the increase in fiber content. However, ductility of the composite decreased with the increase in fiber volume fraction beyond a certain value. In order to achieve enhanced ductility, it is recommended that the UHPC composite attains a minimum strain of 1% at peak stress. Using the reinforcement ratio (0.9%) in the present study, it is recommended to use UHPC with 0.5–0.75% fibers along with A1035 bars.
- For a particular fiber volume fraction and type of rebar, the strain-hardening modulus recorded the maximum value for the composite with parallel fibers and the minimum value for the composite with perpendicular fibers. The value for random fiber orientation was in between.

For future study, it is recommended that the influence of fiber orientation be investigated for UHPC specimens with a wider range of fiber volume fractions and rebar reinforcement ratio.

Author Contributions: Conceptualization, K.W.; methodology, C.H. and M.R.; formal analysis, M.R.; writing–original draft preparation, M.R.; writing—review and editing, K.W. and M.R.; supervision, K.W.

Funding: This research received no external funding.

Acknowledgments: The second author acknowledges the support of HS-STEM fellowship from the Department of Homeland Security, USA. The authors acknowledge the support of LafargeHolcim and the University of Connecticut for this work.

Conflicts of Interest: The authors declare no conflict of interest.

References

1. Damgaard Jensen, A.; Chatterji, S. State of the art report on micro-cracking and lifetime of concrete—Part 1. *Mat. Struct.* **1996**, *29*, 3. [CrossRef]
2. Sigrist, V.; Rauch, M. Deformation behavior of reinforced UHPFRC elements in tension. In *Anonymous Tailor Made Concrete Structures*; CRC Press: Boca Raton, FL, USA, 2008; pp. 405–410.
3. Wille, K.; Kim, D.; Naaman, A.E. Strain-hardening UHP-FRC with low fiber contents. *Mater. Struct.* **2011**, *44*, 583–598. [CrossRef]
4. Jungwirth, J. Zum Tragverhalten von Zugbeanspruchten Bauteilen Aus Ultra-Hochleistungs-Faserbeton. Ph.D. Thesis, École Polytechnique Fédérale de Lausanne, Lausanne, Switzerland, 2006.

5. Huang, H.; Su, A.; Gao, X.; Yang, Y. Influence of formwork wall effect on fiber orientation of UHPC with two casting methods. *Constr. Build. Mater.* **2019**, *15*, 310–320. [CrossRef]
6. Roy, M.; Ray, I.; Julio, F.D. High-Performance Fiber-Reinforced Concrete: Development and Evaluation as a Repairing Material. *J. Mater. Civ. Eng.* **2014**, *26*, 04014074. [CrossRef]
7. Roy, M.; Hollmann, C.; Wille, K. Influence of volume fraction and orientation of fibers on the pullout behavior of reinforcement bar embedded in ultra high performance concrete. *Constr. Build. Mater.* **2017**, *146*, 582–593. [CrossRef]
8. Redaelli, D. Testing of Reinforced High Performance Fibre Concrete Members in Tension. In Proceedings of the 6th International PhD Symposium in Civil Engineering, Zurich, Switzerland, 23–26 August 2006.
9. Leutbecher, T.; Fehling, E. Crack Formation and Tensile Behaviour of UHPC Reinforced with a Combination of Rebars and Fibres. In Proceedings of the Second International Symposium on Ultra High Performance Concrete, Kassel, Germany, 5–7 March 2008; pp. 497–504.
10. Kunieda, M.; Hussein, M.; Ueda, N.; Nakamura, H. Enhancement of Crack Distribution of UHPC-SHCC under Axial Tension Using Steel Reinforcement. *J. Adv. Concr. Technol.* **2010**, *8*, 49–57. [CrossRef]
11. Larusson, L.H.; Fischer, G. Bond Slip and Crack Development in FRC and Regular Concrete Specimens Longitudinally Reinfroced with FRP or Steel under Tension Loading. In Proceedings of the Bond in Concrete 2012: Bond, Anchorage, Detailing—Fourth International Symposium, Brescia, Italy, 17–20 June 2012; pp. 847–854.
12. Deluce, J.; Lee, S.; Vecchio, F.J. Crack Formation in FRC Structural Elements Containing Conventional Reinforcement. In *High Performance Fiber Reinforced Cement Composites 6 (HPFRCC 6)*; Parra-Montesinos, G.J., Reinhardt, H.W., Naaman, A.E., Eds.; Springer: Dordrecht, The Netherlands, 2012; pp. 271–278.
13. Yun, H.D.; Kim, S.W.; Jeon, E.; Park, W.S.; Fukuyama, H. Tension Stiffening and Damage Tolerance of Strain-Hardening Cement Composite (SHCC) Tension Ties Under Monotonic and Repeated Cyclic Loadings. In Proceedings of the 14th World Conference on Earthquake Engineering, Beijing, China, 12–17 October 2008.
14. *Eureka Project EU264*. Compresit, Final Administrative Report, Project Periode: May 1990–December 1993. 1994. Available online: https://books.google.com/books?id=lWNYVrb4MdYC&pg=PA237&lpg=PA237&dq=eureka+project+Compresit,+Final+Administrative+Report&source=bl&ots=lmNeKZfOdM&sig=ACfU3U0Gc-BUfNZNen5BYCX5_ojcdg5_kQ&hl=en&sa=X&ved=2ahUKEwjCq73ZpMbjAhWOjVkKHdIrD2AQ6AEwAHoECAgQAQ#v=onepage&q=eureka%20project%20Compresit%2C%20Final%20Administrative%20Report&f=false (accessed on 22 June 2019).
15. Leutbecher, T. Rissbildung und Zugtragverhalten von mit Stabstahl und Fasern bewehrtem Ultrahochfesten Beton (UHPC). Ph.D. Thesis, University of Kassel, Kassel, Germany, 2007.
16. Sturwald, S.; Fehling, E. Design of Reinforced UHPFRC in Flexure. In Proceedings of the Hipermat 2012, 3rd International Symposium on UHPC and Nanotechnology for High Performance Construction Materials, Kassel, Germany, 7–9 March 2012; pp. 443–450.
17. Leutbecher, T.; Fehling, E. Structural Behavior of UHPC under Tensile Stress and Biaxial Loading. In Proceedings of the International Symposium on Ultra High Performance Concrete, Kassel, Germany, 13–15 September 2004; pp. 435–446.
18. Schumacher, P. Rotation Capacity of Self-Compacting Steel Fiber Reinforced Concrete. Ph.D. Thesis, Delft University of Technology, Delft, The Netherlands, 2006.
19. Habel, K. Structural Behavior of Elements Combining Ultra-High Performance Fibre Reinforced Concretes (UHPFRC) and Reinforced Concrete. Ph.D. Thesis, École Polytechnique Fédérale de Lausanne, Lausanne, Switzerland, 2004.
20. Shionaga, R. Structural Behavior of High Performance Fiber Reinforced Concrete in Tension and Bending. In Proceedings of the 6th International PhD Symposium in Civil Engineering, Zurich, Switzerland, 23–26 August 2006; pp. 142–143.
21. ASTM International. *ASTM A615/A615M-13, Standard Specification for Deformed and Plain Carbon-Steel Bars for Concrete Reinforcement*; ASTM International: West Conshohocken, PA, USA, 2013.
22. ASTM International. *ASTM A1035/A1035M-13b: Standard Specification for Deformed and Plain, Low-Carbon, Chromium, Steel Bars for Concrete Reinforcement*; ASTM International: West Conshohocken, PA, USA, 2013.
23. ASTM International. *ASTM A370-13, Standard Test Methods and Definitions for Mechanical Testing of Steel Products*; ASTM International: West Conshohocken, PA, USA, 2013.

24. Seliem, H.M.; Hosny, A.; Rizkalla, S.; Zia, P.; Briggs, M.; Miller, S. Bond Characteristics of ASTM A1035 Steel Reinforcing Bars. *ACI Struct. J.* **2009**, *106*, 530–539.
25. Roy, M.; Hollmann, C.; Wille, K. Effect of Fiber Orientation on Pullout Behavior of Rebar Embedded in UHPC. In Proceedings of the HiPerMat 2016 4th International Symposium on Ultra-High Performance Concrete and High Performance Materials, Kassel, Germany, 9–11 March 2016.
26. ASTM International. *ASTM C39, Standard Test Method for Compressive Strength of Cylindrical Concrete Specimens*; ASTM International: West Conshohocken, PA, USA, 2011.
27. Moreno, D.M.; Trono, W.; Jen, G.; Ostertag, C.; Billington, S.L. Tension-Stiffening in Reinforced High Performance Fiber-Reinforced Cement-Based Composites under Direct Tension. In *High Performance Fiber Reinforced Cement Composites 6 (HPFRCC 6)*; Parra-Montesinos, G.J., Reinhardt, H.W., Naaman, A.E., Eds.; Springer: Dordrecht, The Netherlands, 2012; pp. 263–270.
28. Otsuka, K.; Mihashi, H.; Kiyota, M.; Mori, S.; Kawamata, A. Observation of Multiple Cracking in Hybrid FRCC at Micro and Meso Levels. *J. Adv. Concr. Technol.* **2003**, *1*, 291–298. [CrossRef]
29. Fantilli, A.P.; Mihashi, H.; Vallini, P. Strain compatibility between HPFRCC and steel reinforcement. *Mater. Struct.* **2005**, *38*, 495–503. [CrossRef]
30. Jungwirth, J.; Muttoni, A. Structural Behavior of Tension Members in UHPC. In Proceedings of the International Symposium on Ultra High Performance Concrete, Kassel, Germany, 13–15 September 2004; pp. 533–544.
31. ACI. *ACI 224R-01, Control of Cracking in Concrete Structures*; American Concrete Institute: Farmington Hills, MI, USA, 2001.